Synthesis, characterization and computational study of nitrogen-doped CeO_2 nanoparticles with visible-light activity

Changjie Mao,[ab] Yixin Zhao,[a] Xiaofeng Qiu,[a] Junjie Zhu*[b] and Clemens Burda*[a]

Received 8th April 2008, Accepted 13th June 2008
First published as an Advance Article on the web 30th July 2008
DOI: 10.1039/b805915b

Nitrogen-doped CeO_2 nanoparticles were synthesized through a wet-chemical route. Nitrogen has been successfully incorporated into CeO_2 nanoparticles and the nitrogen-doping level was also successfully controlled. The optical properties due to the different N-doping levels in CeO_2 nanoparticles were characterized by UV-Vis diffuse reflectance spectroscopy (DRS), which showed a visible-light absorbance shift. The resulting nanoparticles show enhanced visible-light sensitivity and photocatalytic activity compared to undoped CeO_2 nanoparticles. DFT calculations were performed to explore the effect of nitrogen doping *versus* oxygen vacancies. The calculations show that the change of the electronic structure upon N-doping CeO_2 is quite different from that of N-doped TiO_2, which has been studied extensively.

Introduction

Metal oxides photocatalysts have been extensively studied for the utilization of solar light as energy source because of their relatively low cost, high photostability and useful optoelectronic properties.[1–4] However, a major drawback for such metal oxides is that their high band-gap energies limit the utilization of a wider range of the solar spectrum. Many attempts have been made to shift the optical response of such materials from the UV to the visible spectral range, one of the most interesting approaches is doping.[5] Recently, nitrogen received a great deal of attention as a favorable non-metal dopant because of its size similar to oxygen and its relatively small ionization energy.[6–18] To date, the most successful N-doping studies seem to be conducted on only a very limited number of metal oxides, mainly on TiO_2.[7–18] The preparation methods of N-doped metal oxide nanomaterials include wet chemistry, high temperature treatment sintering, and ion implantation.[19] These methods have been successfully used to prepare visible-light active N-doped TiO_2 NPs, which show improved photocatalytic acitivities as catalysts and photoelectrical performances such as materials for solar cells.

Ceria (CeO_2) has important applications in solid oxide fuel cells and oxygen storage components for catalysts because of its unique redox properties.[20,21] In addition it is abundant, has minimal toxicity and low cost, which makes it suitable for optoelectronic and photocatalytic applications. Furthermore, CeO_2 is a wide band-gap semiconducting material which absorbs light in the near UV and slightly in the visible region. These features make cerium dioxide a promising material that can be used in photocatalytic reactions. Bamwenda *et al.* have reported that cerium dioxide is a potential photocatalyst that can be used to decompose water to produce oxygen.[22] It is not until recently, that selective metal doping of CeO_2 to improve its performance started to appear in the literature. Corma *et al.* prepared Zr^{4+}- and La^{3+}-doped nanostructured CeO_2 materials by a wet impregnation method and found their potential use in solar cell devices.[23] Nitrogen doping of ceria holds great potential in enhancing the performance of this material as catalyst. Incorporation of non-metal elements into CeO_2 is still a great challenge. Properly doped and visible-light-sensitive CeO_2 nanoparticles could be useful for solar- and fuel-cell applications. The major obstacle for the studies on the non-metal doping of metal oxides is the lack of reliable methods to incorporate the desired elements with the appropriate amount into the metal oxide matrices. Fuertes *et al.* have doped nitrogen into ceria powder by sintering CeO_2 in NH_3 flow at very high temperature.[24] Recently, we reported the synthesis of group IVB N-doped metal oxide particles with controllable doping levels at the nanoscale through a reliable wet chemical approach, which extended the N-doping strategy to other interesting metal oxides.[25]

Towards this end, we present here the synthesis of N-doped CeO_2 nanoparticles. X-Ray photoelectron spectroscopy (XPS) and optical studies show that N can be doped into the CeO_2 matrix and visible-light absorption of the N-doped CeO_2 nanoparticles is found to be significantly enhanced. Visible-light photocatalytic decomposition of methylene blue indicates that the N-doped CeO_2 nanoparticles are photocatalytically active under visible light, which may make CeO_2 nanoparticles an interesting material for a wider range of applications. The N-doping mechnisms and effects on metal oxides, especially on TiO_2, have been discussed extensively in the literature. Also, experimental characterization including optical measurements and theoretical calculations such as DFT computations have been widely used to help understand the trends of electronic structure changes.[8–10] Even though the absolute values from DFT computations do not match very well with the experimentally obtained ones, DFT calculations are useful for

[a] *Center for Chemical Dynamics and Nanomaterials Research, Department of Chemistry, Case Western Reserve University, 10900 Euclid Avenue, Cleveland, OH 44106, USA. E-mail: burda@case.edu; Fax: +1 (1)216 368 3006; Tel: +1 (1)216 368 5313*
[b] *Key Laboratory of Analytical Chemistry for Life Science Department of Chemistry, Nanjing University, Nanjing, 210093, P. R. China. E-mail: jjzhu@netra.nju.edu.cn; Tel: +86 (0)25 8359 4976*

exploring the trends of electronic structure changes in materials after N-doping and introduction of oxygen vacancies. In this work, a DFT calculation was applied to a simplified CeO_2, $CeO_{2-x}N_x$ and CeO_{2-x} model to help understand the doping and oxygen vacancy effects on the electronic structure of ceria and we compared it to the changes in TiO_2.

Experimental details

Synthesis of N-doped CeO_2 nanoparticles

2 g (5 mmoL) $Ce(Ac)_2{\cdot}H_2O$ (99.9%, Aldrich) and 15 mL ethylenediamine (98%, Strem) were added to 100 mL 1-butanol (anhydrous, Aldrich) under stirring. The solution was refluxed for 24 h to become a yellow-colored solution. The precursor solution was divided into 4 vials (each vial containing 25 mL of precursor solution and used when needed). After the precursor solution was cooled to room temperature; acetic acid was added slowly into these vials to neutralize the excess of ethlyenediamine. The resulting solutions were hydrolyzed by drop-wise addition of 10 mL distilled water. Then, 10 mL of 1M KOH solution was added to the vials to increase the OH^- concentration. Finally, the resulting dispersions were centrifuged and washed with distilled water and ethanol and dried in vacuum. The dried powders were then sintered in air at 200 °C for 45 min.

Characterization

Powder X-ray diffractometry (XRD) was performed on a Scintag X-1 Advanced X-ray diffractometer (2.4° min^{-1}, Cu Kα radiation). The instrumental resolution was determined by using single crystalline alumina as standard. Transmission electron microscopy (TEM) was measured on a JEOL 1200CX (accelerating voltage: 80 kV). X-ray photoelectron spectra (XPS) were obtained on a PHI ESCA-5600 XPS system (Al K X-ray source, 5×10^{-8} Pa), choosing C 1s (284.6 eV) as the reference line. The UV-Vis diffuse reflectance spectroscopy (DRS) was recorded on a Varian Cary Bio 50 UV-Vis spectrometer equipped with a BarrelinoTM remote diffuse reflection probe (Harrick Sci. Co.), choosing MgO powders as a reference standard. The difference DRS spectra ($\Delta\rho$) were plotted to show the reflectivity changes of the spectra. $\Delta\rho$ were calculated by ρ_{mnx} (mn = N-doped CeO_2 x = different N-doping level) subtracting DRS spectra of undoped CeO_2 ρ_{m0} (m = CeO_2). Then $\Delta\rho = \rho_{m0} - \rho_{mnx} > 0$ was obtained and normalized and plotted *vs.* wavelength. The difference absorption spectra show enhancement of absorption through doping.

The photocatalytic activity of N-doped and undoped CeO_2 were evaluated using the photodegradation of methylene blue solution under visible light above 500 nm combined with 150 W high-pressure Xe lamp and a 500 nm long-pass optical filter.[28] The decomposition of methylene blue was monitored by measuring the decolorization of methylene blue in solution at 680 nm. The UV-Vis absorption spectra were recorded on a Varian Cary Bio 50 UV-Vis spectrometer.

Calculation

Bulk crystalline CeO_2 has a fluorite structure, with each Ce^{4+} cation coordinated to eight equivalent O^{2-} ions in a cube, and each O^{2-} anion tetrahedrally coordinated to four Ce^{4+} ions. We use the experimental value 5.411 Å as lattice parameter. In this study, a conventional 12-atom cubic unit cell of CeO_2 was used as a simplified CeO_2 model. N-Doped CeO_2 was then modeled by introducing one N-doping atom to substitute one O atom in the cell, The doped system was assumed to keep the cubic structure and the cell parameter and atomic positions were optimized, giving virtually no change in the unit cell. The oxygen vacancy model is created by taken an O atom from the lattice, which is based on the CeO_2 experimental structure without further geometry optimization.

The computations have been performed at the DFT level using the plane-wave-pseudopotential approach, together with the Perdew–Burke–Ernzerhof (PBE) exchange correlation functional and ultrasoft pseudopotentials, the energy cutoff was chosen at 370 eV.

Results and discussion

The phase purity and size of the products were studied by X-ray powder diffraction (XRD), while the morphologies of the particles were examined by transmission electron microscopy (TEM). The X-ray diffraction (XRD) of the obtained products is shown in Fig. 1a. It was found that as-synthesized CeO_2 nanoparticles show good crystallinity even before sintering, while other metal oxides like TiO_2 synthesized by wet methods are amorphous before sintering.[25,29] All diffraction peaks can be indexed to the fluorite cubic phase of ceria with the lattice constants a = 5.411 Å, which are in good agreement with the JCPDS card no. 43-1002. It is found that diffraction peaks become sharper and narrower with increasing sintering temperature, indicating the improvement of crystallinity and growth of the particle size. However, the N concentration characterized by XPS has indicated that as the sintering temperature exceeds 400 °C, the resulting N-doping levels become lower than 1% atomic ratio, indicating that the replacement of nitrogen with oxygen may occurs in air at elevated temperatures. It was found that the samples sintered under 200 °C maintain both the high N-doping levels and the photocatalytic properties. Therefore, the sintered samples used for later catalytic measurements in this study were post-preparatively sintered at 200 °C in air. From the full width at half maximum (FWHM) of the three most intensive peaks in the XRD pattern, the average crystallite size of N-doped CeO_2 is 4 nm evaluated according to the Scherrer equation. Fig. 1b shows a typical TEM image of N-doped CeO_2 nanoparticles. It can be seen that the nanoparticles size is in the range of 2 nm to 10 nm and the shape of the particles is mostly spherical. The size obtained from TEM matches well with the crystal size from the XRD data when calculated with the Scherrer equation. These results show that the N-doped CeO_2 nanoparticles prepared through this method can be restricted to a sub-10 nm region, which is the size range where good surface-to-volume ratios can be achieved for efficient surface catalysis.

In order to further study the doping level and chemical environment of the elements in the nanoparticles, core level X-ray photoelectron spectroscopy (XPS) was applied to evaluate the effectiveness of the N-doping into the CeO_2 through this method.

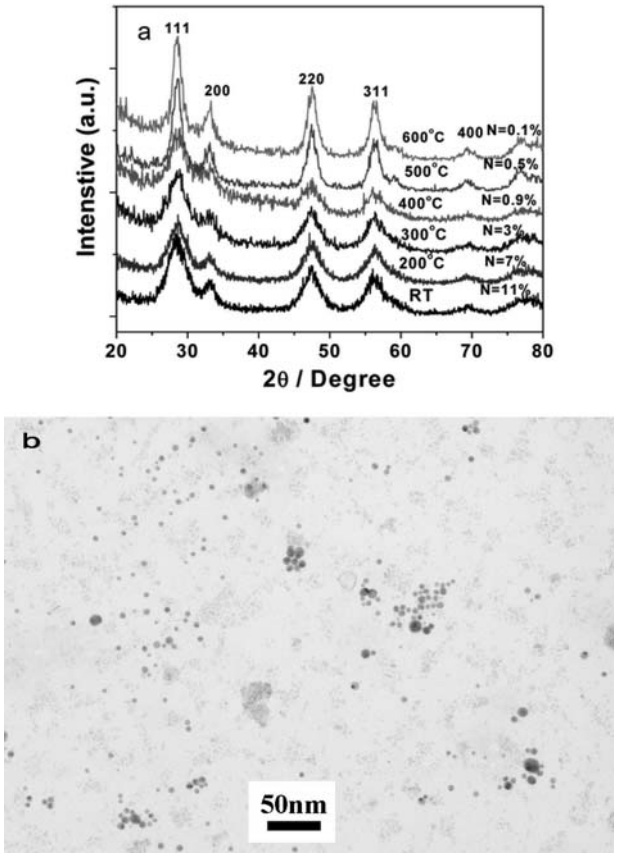

Fig. 1 (a) XRD patterns for CeO_2 and N-doped CeO_2 at different sintered temperatures. (b) TEM image of N-doped CeO_2.

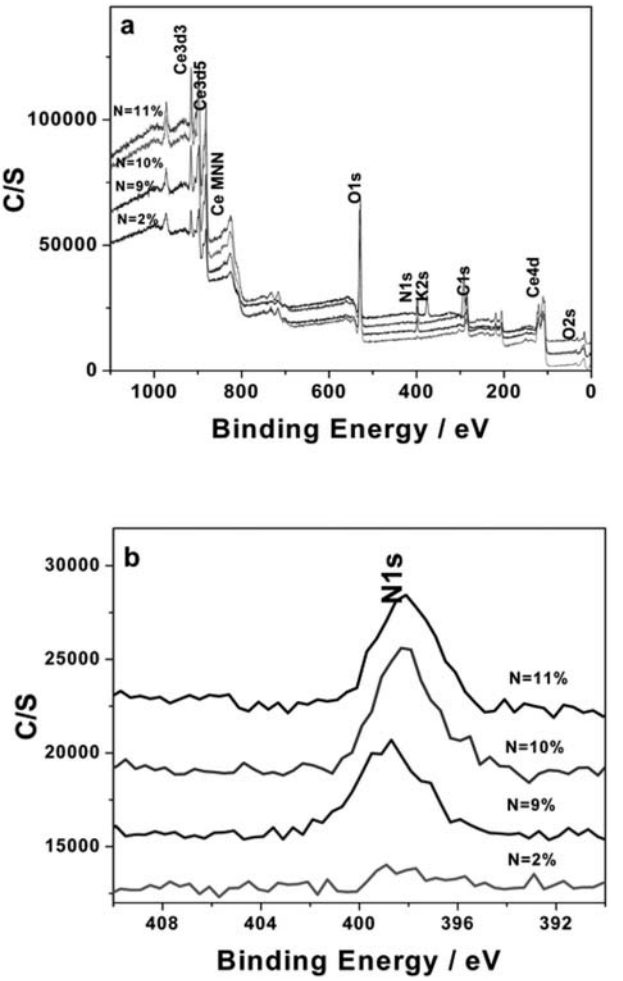

Fig. 2 The full scale XPS spectra of $CeO_{2-x}N_x$ nanoparticles with different N-doping levels. Fig. 2b contains the enlarged N 1s regions of the corresponding full scale XPS spectra.

In Fig. 2, full-scale XPS spectra of CeO_2 with different N-doping levels were plotted from bottom to top with increasing N-doping level. The binding energy was calibrated with respect to C 1 s energy at 284.6 eV.

All of these spectra show very clear CeO_2 features and an additional N 1s signal around 398 eV, which indicates that N is successfully incorporated into CeO_2. The binding energy of N 1s electrons obtained here is relatively lower than that found in the N-doped TiO_2 nanoparticles prepared with a similar method, which appears around 399.1 eV. This is due to the central metal ion Ce(IV), which is electron richer than Ti(IV). Therefore, the electron density around N in the CeO_2 matrix is higher than that in the TiO_2 matrix. This result also shows that the doped N is sufficiently affected by the surrounding metal ions. Fuertes *et al*. reported an N peak for their N-doped ceria identified at 400.1 eV, which is assigned as the chemisorbed nitrogen, and 397.4 eV, which is assigned as the formation of Ce–N bond.[24] The XPS electron binding energy of the Ce $3d_{5/2}$electron is in the range of 915.1–915.9 eV, while in pure CeO_2 the binding energy is reported at 916.7 eV. The observed lowered $3d_{5/2}$ binding energy indicates that the replacement of O with N in the matrix reduces the binding energy due to the lower electronegativity of N compared to oxygen. The reduced Ce $3d_{5/2}$ binding energy also proves that the N-dopant was efficiently incorporated into the metal oxide matrix. Fig. 2b shows the expanded N 1s regions of the N-doped CeO_2 at different N levels. All of the N 1s peaks range from 394 to 402 eV and are centered around 398 eV. The XPS spectra show that the N-doping levels can be controlled by the amount of acid (acetic acid) or base (KOH) added during the hydrolysis. The spectra are plotted from top to bottom for increasing acetic acid and KOH addition. Generally, the N-doping levels decrease with the increase of acid addition during the hydrolysis. While the addition of KOH during hydrolysis increases the N-doping level in the resulting nanomaterials. It appears that higher acetic acid concentrations during the hydrolysis result in the replacement of amino- groups by CH_3COO^-, which decrease the N-doping level in the product. The XPS spectra confirm that by controlling the hydrolysis conditions, $CeO_{2-x}N_x$ nanoparticles with different N-doping levels can be achieved.

UV-Vis diffuse reflectance spectroscopy (DRS) was used to evaluate the optical properties of the N-doped and pure CeO_2 nanoparticles. The pure CeO_2 nanoparticles without doping show an onset of absorption at 395 nm, which corresponds to the band-gap energy of 3.1 eV. This value is consistent with other reported values from 2.8–3.2 eV.[22] DRS spectra of $CeO_{2-x}N_x$ nanoparticles with different N-dopant concentrations are shown in Fig. 3a. The DRS spectrum reveals that N-doped CeO_2 shows significantly increased absorption in the

visible light region. It is also observed that with the increase of N-doping levels, the absorption of N-doped CeO_2 experiences a red shift. The results show that the increase of N content in CeO_2 enhances the visible-light absorption. Similar phenomena were also observed in N-doped TiO_2, ZrO_2 and HfO_2 nanoparticles.[25] It is reported that in the N-doped TiO_2 case the absorption <500 nm is due to the additional states brought by the N near the valence band edge, while the absorption >500 nm is explained with doping-induced defects and oxygen vacancies.[26–30] We believe that this explanation is also applicable for the N-doped CeO_2 nanoparticles.

To further explore the causes for the visible-light absorption, a recently introduced difference DRS analysis[27–30] was applied in this study. The difference DRS spectra demonstrate the treatment-induced spectral changes. Fig. 3b shows the difference DRS spectra of $CeO_{2-x}N_x$ nanoparticles. Compared to TiO_2, ZrO_2 and HfO_2 nanoparticles, very similar spectra were observed in the $CeO_{2-x}N_x$ nanoparticles spectra. Regardless of the N-doping level, the absorbance edges of differently doped CeO_2 nanoparticles seem to change very little around 400 nm in the spectra, while the absorption above 500 nm differ more

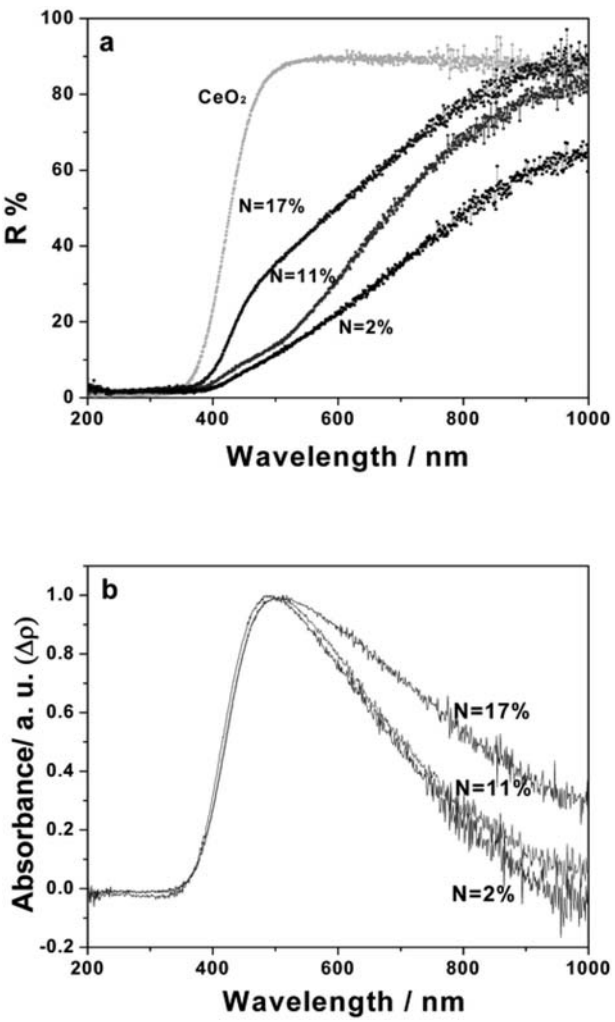

Fig. 3 UV-Vis diffuse reflectance spectra (DRS) (a) and difference DRS spectra (Δρ) (b) of $CeO_{2-x}N_x$ nanoparticle powders.

significantly between the CeO_2 nanoparticles with different N-doping levels. This observation indicates that the N-doping may cause similar effects on the density of states close to the valence band edge, while causing more pronounced changes to the defects states and oxygen vacancies. In fact, the N-doping sites also act as oxygen vacancies. Thus, the number of oxygen vacancies is expected to be more pronounced with increasing N-doping level.[15–17,28,30] The difference DRS spectra in Fig. 3b clearly show the change of these oxygen vacancies as a function of N-doping levels in the CeO_2 case.

To investigate the influence of N-doping on the electronic structure of the CeO_2 matrix, a widely used DFT calculation was carried out to show the changes of the electronic structure due to the dopant incorporation.[8,15,26,31] The density of states (DOS) of the fluorite-type CeO_2 crystal with two kinds of manipulations were calculated. The first one is the replacement of an oxygen atom by an N atom, as shown in Fig. 4, which is fully geometry-optimized. The second one is creating an O vacancy within the lattice, which is based on the CeO_2 experimental structure without further geometry optimization. The DFT calculations show that in both cases, the transitions appear at lower energy due to introducing intragap energy levels by impurity doping or vacancies compared to the pure CeO_2. However, the valence-band (VB) edges in these cases did not shift up like those in TiO_2 but towards negative energies.[8,26] On the other hand, the conduction-band (CB) edges were significantly lowered. Therefore, an overall lowering in transition energy was found after the introduction of N-doping or oxygen defects. However, the VB edges in these CeO_2 calculations did not shift up like those in TiO_2 but towards negative energies.[8,26] The DFT calculation studies on N-doping and oxygen vacancies on TiO_2 revealed that the N-dopants introduce energy levels above the O 2p VB edge. Whether the conduction band edge effectively shifts depends on the doping model and the different calculation methods.[8,15,26,31] To make a clear comparison, we adopt the same method and same model for the calculation of the N-doped anatase TiO_2. A 24 atom TiO_2 supercell model with unit cell parameters $a = 3.776$ Å and $c = 9.486$ Å was used as the calculation model and an O atom was replaced with the N atom as shown in Fig. 4b. The calculation details are the same as in the calculations for the CeO_2 system. The results for the N-doping TiO_2 show the valence band has shifted upward to the conduction band compared to the pure TiO_2, which is consistent with other earlier results.[8,26] The conduction band of the N-doped TiO_2 shifted towards the valence band as shown in earlier calculations.[8] However, the magnitude of the shift is larger than previously reported, which may come from simplification of our model with only 24 atoms in the supercell while others used up to 96 atoms per cell. The consistency of our N-doping TiO_2 calculation with previous work indicated that our DFT calculation model and methodology for the CeO_2 system are useful and reliable. Indeed, they exhibit similar behavior as reported in the DFT calculation of Yang *et al.* on CeO_2 with oxygen vacancies.[31] On the other hand, the conduction-band (CB) edges were significantly lowered. Therefore, an overall lowering in transition energy was found after the introduction of N-doping or oxygen defects.

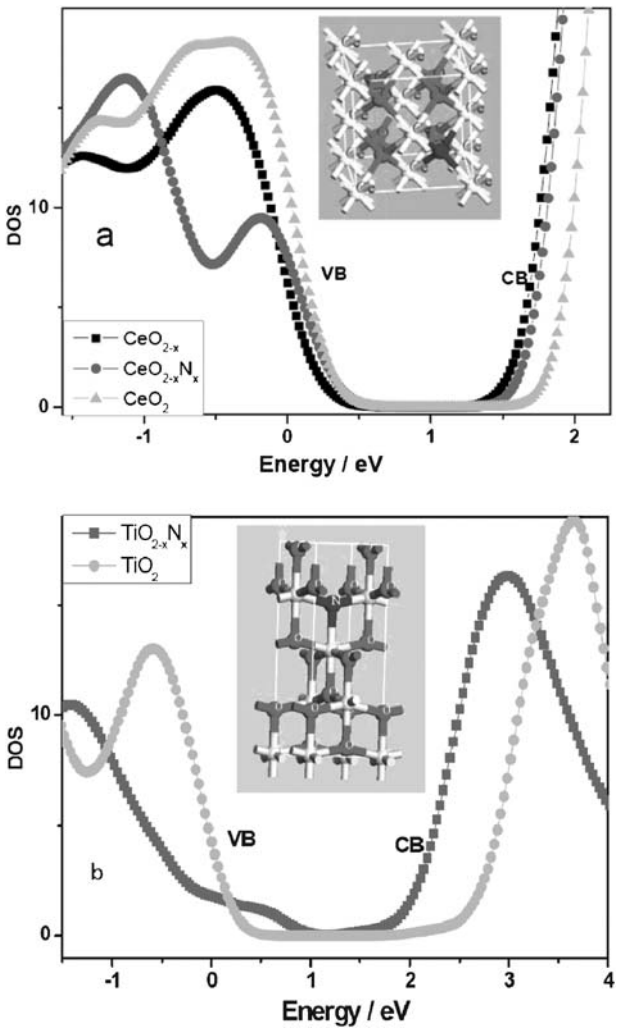

Fig. 4 DFT calculations of the densities of states of fluorite-type CeO_2 with substituted oxygen sites as indicated in the inset.

This suggests that both the N-doping and the doping-induced oxygen vacancies may cause the visible-light sensitivity of $CeO_{2-x}N_x$ nanoparticles. However, the band edges are lowered on the both sides of the energy gap. This may lead to an increased photooxidation potential, but on the other hand to a lowered photo-reduction potential. Therefore, the redox chemistry of this photocatalyst could be different from that of nitrogen-doped titania nanoparticles reported earlier. To evaluate the light-induced performance of the N-doped CeO_2, a standard methylene blue photobleaching measurement under visible light irradiation was performed.[8,9,29–33]

The photoactivity of undoped CeO_2 nanoparticles was also measured as a reference to that of the synthesized doped materials. Fig. 5 shows the optical density change of a methlyene blue solution at 680 nm in the presence of $CeO_{2-x}N_x$ nanoparticles as a function of time upon 500 nm excitation. It is found that the N-doped CeO_2 nanoparticles show a higher photocatalytic activity compared to pure CeO_2 particles. On the other hand, we found that the N-doping level does not affect the photocatalytic activities of N-doped CeO_2 drastically. However, best decomposition rates were observed for doping concentrations at ~4%.

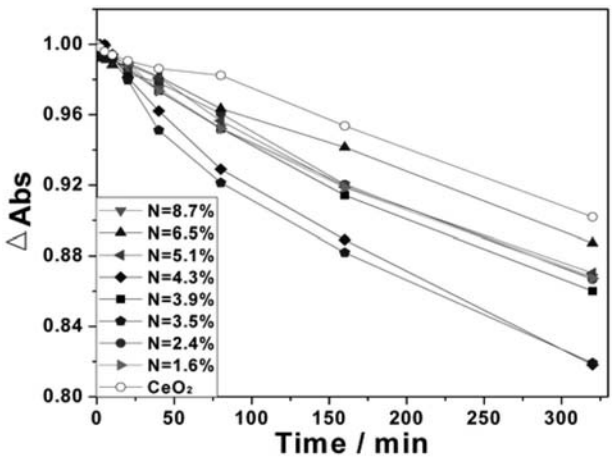

Fig. 5 Methylene blue photodecomposition catalyzed by $CeO_{2-x}N_x$ nanoparticles upon photoexcitation with wavelength >500 nm.

An explanation for this observation could be that by increasing doping above ~4% the defect-induced carrier recombination outweighs the benefit of the better optical properties.[34]

Conclusion

We successfully synthesized a series of nitrogen-doped CeO_2 nanoparticles with different N-doping levels through a wet-chemical method. The XRD and TEM results indicated that the synthesized $CeO_{2-x}N_x$ nanoparticles are of fluorite cubic crystal structure with sub-10 nm size. A core level XPS study shows that N was effectively incorporated into the CeO_2 matrix, and the N-doping has changed the electronic structure of the ceria nanoparticles, as indicated by the observed lowered $3d_{5/2}$ binding energy. DRS and difference DRS spectra show that N-doping can significantly affect the absorption of CeO_2 nanoparticles. Visible-light induced methylene blue decomposition measurements suggest that N-doping can help to enhance the photocatalytic performance of CeO_2 nanoparticles.

This study shows that the wet-chemical method developed can efficiently dope metal oxides with varying amounts of nitrogen. The N-doping procedure can significantly change the physical and chemical properties of metal oxides, which provides scientists with a promising method to modify the electronic structure of metal oxides, and thus can extend their range of applications.

Acknowledgements

CB acknowledges the financial support from the NSF (#CHE-0239688), and ACS-PRF (#45359-AC10). The authors would like to thank S. F. Li for help with calculations. JJZ is financially supported by the National Natural Science Foundation of China (Nos. 20635020, 20325516) and CJM is grateful for a Visiting Scholarship from the China Scholarship Council. We acknowledge funding from NSF-NIRT (#0608896).

References

1 M. Grätzel, *Nature*, 2001, **414**, 338.
2 A. L. Linsebigler, G. Lu and J. T. Yates, Jr, *Chem. Rev*., 1995, **95**, 735.
3 C. Santato, M. Ulmann and J. Augustynski, *Adv. Mater*., 2001, **105**, 936.
4 A. Duret and M. Gratzel, *J. Phys. Chem. B*, 2005, **109**, 17184.
5 U. Diebold, *Surf. Sci. Rep*., 2003, **48**, 53.
6 C. H. Park, S. B. Zhang and S. H. Wei, *Phys. Rev. B: Condens. Matter Mater. Phys*., 2002, **66**, 732021.
7 S. Sato, *Chem. Phys. Lett*., 1986, **123**, 126.
8 R. Asahi, T. Morikawa, T. Ohwaki, K. Aoki and Y. Taga, *Science*, 2001, **293**, 269.
9 C. Burda, Y. B. Lou, X. B. Chen, A. C. S. Samia, J. Stout and J. L. Gole, *Nano Lett*., 2003, **3**, 1049.
10 S. Sakthivel and H. Kisch, *ChemPhysChem*, 2003, **4**, 487.
11 T. Umebayashi, T. Yamaki, S. Yamamoto, A. Miyashita, S. Tanaka, T. Sumita and K. Asai, *J. Appl. Phys*., 2003, **93**, 5156.
12 H. Irie, Y. Watanabe and K. Hashimoto, *J. Phys. Chem. B*, 2003, **107**, 5483.
13 R. Nakamura, T. Tanaka and Y. Nakato, *J. Phys. Chem. B*, 2004, **108**, 10617.
14 S. Sakthivel, M. Janczarek and H. Kisch, *J. Phys. Chem. B*, 2004, **108**, 19384.
15 C. D. Valentin, G. Pacchioni and A. Selloni, *J. Phys. Chem. B*, 2004, **70**, 851161.
16 J. Lee, J. Park and J. Cho, *Appl. Phys. Lett*., 2005, **87**, 119041.
17 Z. Lin, A. Orlov, R. M. Lambert and M. C. Payne, *J. Phys. Chem. B*, 2005, **109**, 20948.
18 J. L Gole, J. D. Stout, C. Burda, Y. B. Lou and X. B. Chen, *J. Phys. Chem. B*, 2004, **108**, 1230.
19 X. B. Chen and S. S. Mao, *Chem. Rev*., 2007, **107**, 2891.
20 A. Trovarelli, *Catal. Rev. Sci. Eng*., 1996, **38**, 439.
21 A. Trovarelli, *Catalysis by Ceria and Related Materials*, World Scientific Publishing Company, Singapore, 1st edn, 2002.
22 G. R. Bamwenda and H. Arakawar, *J. Mol. Catal. A: Chem*., 2000, **161**, 105.
23 A. Corma, P. Atienzer, H. Garcia and J. Y. Chang-ching, *Nat. Mater*., 2004, **3**, 394.
24 A. B. Jorge, J. Fraxedas, A. Cantarero, A. J. Williams, J. Rodgers, J. P. Attfield and A. Fuertes, *Chem. Mater*., 2008, **20**, 1682.
25 X. F. Qiu, Y. X. Zhao and C. Burda, *Adv. Mater*., 2007, **19**, 3995.
26 Z. S. Lin, A. Orlov, R. M. Lambert and M. C. Payne, *J. Phys. Chem. B*, 2005, **109**, 20948.
27 V. N. Kuznetsov and M. G. Malkin, *J. Appl. Spectrosc*., 2000, **67**, 763.
28 V. N. Kuznetsov and N. Serpone, *J. Phys. Chem. B*, 2006, **110**, 25203.
29 Y. X. Zhao, X. F. Qiu and C. Burda, *Chem. Mater*., 2008, **20**, 2629.
30 N. Serpone, *J. Phys. Chem. B*, 2006, **110**, 24287.
31 Z. X. Yang, G. X. Luo and Z. S. Lu, *J. Chem. Phys*., 2007, **127**, 074704-1.
32 S. M. Prokes, J. L. Gole, X. B. Chen, C. Burda and W. E. Carlos, *Adv. Funct. Mater*., 2005, **15**, 161.
33 X. B. Chen, Y. B. Lou, A. C. S. Samia, C. Burda and J. L. Gole, *Adv. Funct. Mater*., 2005, **15**, 41.
34 M. K. Nowotny, L. R. Sheppard, T. Bak and J. Nowotny, *J. Phys. Chem. C*, 2008, **112**, 5275.